Received 9 June 2017; revised 2 July 2017; accepted 28 July 2017. Date of publication 7 August 2017;
date of current version 23 August 2017. The review of this paper was arranged by Editor A. Nathan.

Digital Object Identifier 10.1109/JEDS.2017.2736538

Dynamic Properties of Flat-Panel X-Ray Image Sensors With Mercury Iodide Photoconductors Undergoing Repeated X-Ray Irradiation

JAE CHUL PARK[1] AND SEUNG-EON AHN[2]

1 Institute of Physics and Applied Physics, Yonsei University, Seoul 03722, South Korea
2 Department of Nano-Optical Engineering, Korea Polytechnic University, Siheung 15073, South Korea

CORRESPONDING AUTHOR: S.-E. AHN (e-mail: seahn@kpu.ac.kr)

ABSTRACT A screen-printed mercury iodide (HgI_2) photoconductor for digital tomosynthesis exhibits considerably reduced signals when subjected to consecutive exposures to X-ray irradiation. This behavior accounts for the trapping of charges generated on previous X-ray shots near the HgI_2/electrode interface. These trapped charges create the conditions that deter subsequent charges generated by the next X-ray shot from traveling from the photoconductor into the electrode. Such conditions can be improved significantly by switching the bias polarity of the photoconductor with an illuminating light under the image sensor. In addition, the signal-to-noise ratio (SNR) is optimum when the duration of the illuminating light is 1 s longer than the applied time of the positive bias. Increases in the bias switching/lighting combination time for obtaining the best SNR are required with increasing amounts of incident X-ray exposure. Such results obtained from making adjustments in the technique for using screen-printed HgI_2 photoconductors for digital tomosynthesis indicate promising results for improving the diagnostic accuracy of this digital imaging method for breast cancer screening while mitigating patients' X-ray exposure.

INDEX TERMS Mercury iodide photodonductor, X-ray image sensor.

I. INTRODUCTION

The appearance of digital X-ray image sensors and their replacement of traditional photographic film brought significant changes to various fields of medical X-ray imaging such as radiography, mammography, fluoroscopy, and angiography [1]–[3]. These digital sensors offer the advantages of immediate image acquisition, high image quality, elimination of costly film processing steps, and easy storage of images [4]–[6]. In the years since the development of these sensors, numerous studies have researched options for achieving enhanced performance. Detective quantum efficiency (DQE), the most important parameter for evaluating the performance of medical X-ray image sensors, is expressed by [6]

$$DQE = \frac{SNR_{OUT}}{SNR_{IN}},$$

where SNR_{OUT} is the signal-to-noise ratio of pixel signals in the image sensor and SNR_{IN} is the signal-to-noise ratio of incident X-ray photons following a Poisson distribution [7], [8]. In other words, DQE can be improved as SNR_{OUT} is increased. The SNR_{OUT} is defined, in general, as the ratio of the mean value S to the standard deviation σ of the pixel-signal values across the image sensor [9]. Thus,

$$SNR = \frac{S}{\sigma}, \tag{1}$$

From this point onward in this letter, SNR is taken to represent SNR_{OUT}. SNR is influenced mainly by X-ray sensitivity and the electrical noise of the X-ray-photoconductive material in the image sensor. An amorphous selenium photoconductor was developed commercially for the direct conversion X-ray image sensor and then various types of photoconductors were intensively researched [10]–[13].

Digital tomosynthesis, which can provide increasingly precise images of breast cancer tumors by taking multiple X-ray images at various angles, requires photoconductors with stable and high SNR values under continuous X-ray

exposure because of the increased exposure of patients to the injected X-rays [14]. The most promising candidate for such photoconductors is mercury iodide (HgI_2) because its X-ray conversion properties, such as mobility, carrier lifetime and electron–hole pair creation energy, are relatively superior to other materials as well as selenium and can be fabricated inexpensively by screen-printing processes [15]. Few studies, however, have researched the dynamic SNR characteristics of screen-printed HgI_2 photoconductors under sequential X-ray exposure. In this paper, we study the degradation mechanism of signals and approaches for improving the dynamic SNR properties of screen-printed HgI_2 photoconductors.

II. EXPERIMENT AND DISCUSSION

Figure 1(a) shows the pixel circuit of an X-ray image sensor. This sensor comprises two major sections: the HgI_2 photoconductor that converts X-rays into electrical charges and the electrical circuitry that transfers the charges to an external charge amplifier. The electrical circuit consists of a storage capacitor that stores charges generated in the photoconductor and an amorphous silicon (a-Si) thin-film transistor (TFT) that transfers charges in the storage capacitor to the external amplifier [16]. Figure 1(b) shows the top view of an optical microscope image of a pixel. The pixel size is 78 μm × 78 μm with a fill factor of 85%; the capacitance of the storage capacitor is 0.58 pF.

The inset of Fig. 1 (b) also shows an indium tin oxide (ITO) layer used as the bottom electrode of an X-ray image sensor. Figure 1(c) shows the cross-sectional scanning electron microscope (SEM) image of a fabricated X-ray image sensor. A 150-μm-thick HgI_2 photoconductor was coated by screen printing on the ITO bottom electrode of a TFT glass substrate. HgI_2 appears here as polycrystalline particles embedded in the polymer binder matrix. The HgI_2 particles were mixed with a polyvinyl butyral organic binder and butyl cellosolve solvent and then evenly dispersed in the binder by three-roll milling process. Finally, a molybdenum thin film as a top electrode was sputtered, and parylene as a passivation layer was deposited by a thermal evaporator. The X-ray image was taken at an energy of 28 keV, with exposures of 0.2, 0.4, 0.8 mGy, and the distance between the source and image sensor was 60 cm.

Figure 2(a) shows a timing diagram for the operation of the sensor depicted in Fig. 2(b). In this scheme, "Idle" refers to the step in which the filament in the X-ray tube is preheated for electron emission. "Precharge" is the operating step in which the storage capacitor is precharged to the reference voltage V_{REF} of the charge amplifier through the TFT, and then the TFT is turned off. "X-ray radiation" is the step in which electrons generated in the photoconductor are stored in the storage capacitor as the X-ray is irradiated. In the "Scan" step, the electron signal charges in the storage capacitor are transferred to the amplifier in the external control board as the TFT is turned on. Figure 2(b) shows the photocurrent, dark current and signal variation according to the number of consecutive X-ray irradiations when the top electrode of the

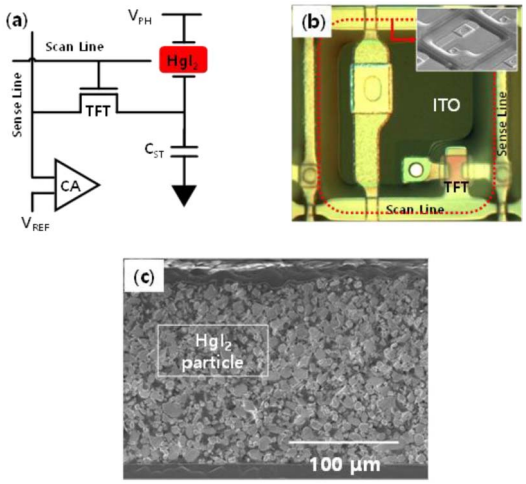

FIGURE 1. (a) The pixel circuit, (b) top view imaged by an optical microscope, and (c) the cross-sectional SEM image of a flat-panel X-ray image sensor of an HgI_2 photoconductor. The red arrow in Fig. 1(c) indicates an HgI_2 particle embedded in the binder.

photoconductor has applied to it a voltage of -70 V at all steps of the operation. The signal in here is value subtracted dark current from photocurrent. The signal shows the same behavior as the photocurrent because there was no change in the dark current in terms of consecutive X-ray shot. The signal sharply decreased in the early stage and then slowly decreased as more X-rays accumulated. This degradation is caused by traps in the photoconductor. The electron–hole pairs generated by incident X-rays drift towards the bottom electrode for electrons and the top electrode for holes under the influence of a negative bias applied to the top electrode. Most of the electrons contribute to signal S of the SNR exiting the photoconductor, but others are trapped at trap sites on the HgI_2/binder and HgI_2/ITO interfaces. Because these trap charges generate negative internal fields near the interface, the electrons of the next irradiation experience difficulty in moving to the bottom electrode. Thus, as the accumulating X-ray dose causes more electrons to be trapped, the signal gradually decreases. Discovering the input energy required to eliminate these trap charges requires examining the activation energy of 1.02 eV, measured from the Arrhenius plot shown in Fig. 2(c) [17]. Thus,

$$D = D_O \exp\left(-\frac{\Delta E}{kT}\right), \tag{2}$$

where D is the dark current and ΔE is the activation energy.

The introduction of light/bias switch-combined techniques enabled the effective removal of electrons trapped during the prior exposure. The voltage applied to the top electrode of the photoconductor was switched from negative to positive in coordination with illuminating a light-emitting diode (LED) under the TFT glass substrate only at the precharge step, as shown in Fig. 3(a). The exponentially sharp decrease in signal strength with increasing exposure counts, as shown in Fig. 2(b), disappeared—surprisingly—as shown in Fig. 3(b).

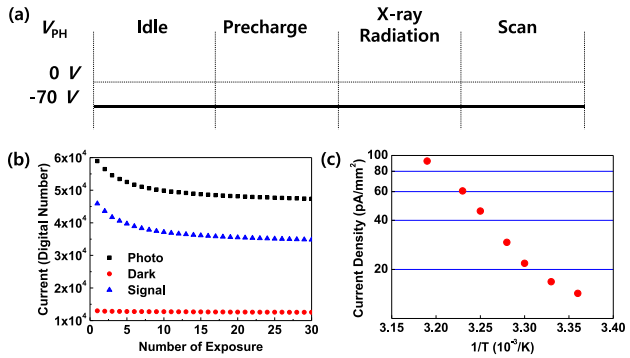

FIGURE 2. **(a) The conventional operating scheme of a flat-panel X-ray image sensor. (b) The photocurrent, dark current and signal variation as a function of the accumulated X-ray exposure. The amount of injected X-rays is 0.2 mGy at the radiation step. (c) The plot of dark current as a function of the reciprocal temperature. The activation energy is extracted from the slope of the curve plotting dark current as a function of the reciprocal temperature.**

This change in behavior offers an explanation for why the trapped electrons were easily excited by the photon energy of the LED and then either swept away from the trap sites on the bottom interface and onto the top electrode or removed to recombine with hole by means of the positive bias of the top electrode. The slow decrease exhibited by the signal until the number of exposures reached 100 was caused by residual traps of the HgI_2/binder interface situated deep within the photoconductor where LED illumination could not penetrate. There was no effect according to the intensity of LED. The standard deviation also decreased considerably and remained almost constant as the accumulated exposure to X-ray increased. Thus, this paper's research shows no significant effects attributable to the intensity of the LED.

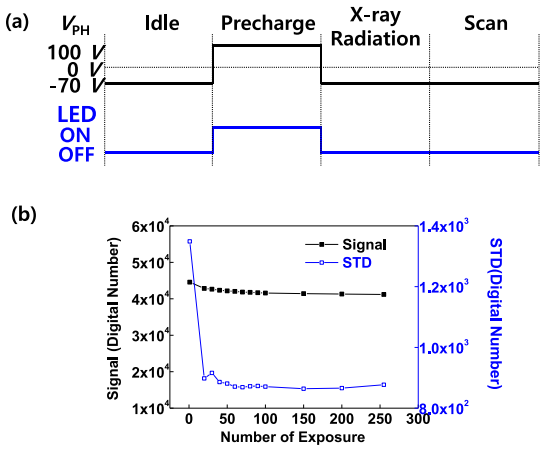

FIGURE 3. **(a) The revised operations scheme for reducing signal degradation. The voltage of the top electrode changes from −70 V to +100 V while illuminating with a light intensity of 3000 cd/m^2 at the precharge step. (b) The signal and standard deviation (STD) as functions of the accumulated X-ray exposure. The X-rays injected at the radiation step measured 0.2 mGy.**

Various combinations of light and bias switch times were tested to enhance the SNR further. Figure 4(a) shows

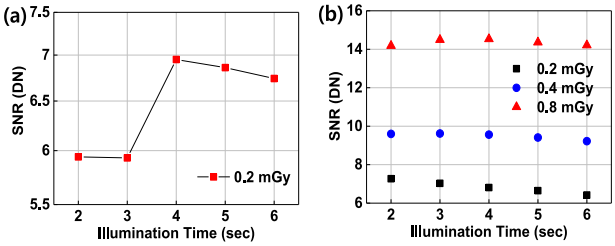

FIGURE 4. **a) The SNR curve as a function of illumination time for the X-ray exposure of 0.2 mGy. The duration time of the positive voltage is 3 s at all measurement points. (b) The SNR curve as a function of illumination time for X-ray exposures of 0.2, 0.4, and 0.8 mGy. The duration time of the positive voltage is 1 s shorter than the illumination time at all measurement points. DN indicates digital number.**

measures of SNR as a function of LED illumination time with a positive bias time fixed at 3 s. The other conditions of this arrangement included light intensity of 3000 cd/m^2, positive bias of 100 V, and X-ray exposure of 0.2 mGy at the radiation step. The LED was illuminated under a glass substrate for 2 s to 6 s at an interval of 1 s per frame. The SNR did not change until the illumination time reached 3 s and then sharply increased when the illumination time reached 4 s. These results show that the SNR was abruptly enhanced when the bias switch time was 1 s shorter than the light time. The same phenomena appeared under the other sets of conditions. The bias polarity was switched again. Then longer illumination times suppressed the hole traps at the bottom interface, thereby increasing the possibility of recombination or erasure out of the electrodes.

Figure 4(b) shows values of the SNR when the X-ray exposures were 0.2, 0.4, and 0.8 mGy at the radiation step. Illumination times of 2, 3, and 4 s for X-ray exposures of 0.2, 0.4, and 0.8 mGy yielded the highest values of SNR: 7.27, 9.62, and 14.53, respectively. The bias time was 1 s shorter than the illumination time under all measurement conditions. The best illumination time increased with increasing doses of incident X-rays. These results illustrate both that trapped electrons increase together with increasing amounts of incident X-ray exposure and that more time is needed to remove these trapped electrons.

III. CONCLUSION

In conclusion, digital tomosynthesis recently has undergone developments intended to enhance the accuracy of images used to diagnose breast cancer. The utility of this advanced imaging technique depends on minimizing the decline in image quality of consecutive X-ray shots. The dynamic properties of screen-printed HgI_2 photoconductors were researched to pursue better techniques to minimize that decline in image quality. This photoconductive material, when subjected to continuous X-ray exposure, showed a 25% reduction in electrical signals in comparison to its initial value. After applying the bias/light-combined technique, a signal variation showing only a 5% reduction represented a discernable improvement in performance. In summary, we

note that electrons are trapped near the HgI_2/ITO interface during the radiation step and that an internal negative field occurs there. The presence of this field hinders the movement of electrons generated at the next radiation step from the photoconductor into the bottom electrode. Thus, the electrical signal of the image sensor continuously decreases. This degradation was effectively reduced, however, by the bias/light-combined operation technique. Our results also showed that the best SNR condition occurred, in most cases, when the light time was 1 s longer than the positive bias-switching time. As the number of X-ray photons injected into the photoconductor rises, the optimal bias/light combination time also increases.

The results of this study indicate that making adjustments in the technique for employing screen-printed HgI_2 photoconductors in the practice of digital tomosynthesis show encouraging results that point to practical ways to heighten the diagnostic accuracy of this digital imaging method for conducting breast cancer screening in ways that achieve attainable goals for minimizing patients' exposure to irradiation through diagnostic X-rays.

REFERENCES

[1] A. Varghese *et al.*, "Radiation doses and estimated risk from angiographic projections during coronary angiography performed using novel flat detector," *J. Appl. Clin. Med. Phys.*, vol. 17, no. 3, pp. 433–441, May 2016, doi: 10.1120/jacmp.v17i3.5926.

[2] W. Zhao, W. G. Ji, A. Debrie, and J. A. Rowlands, "Imaging performance of amorphous selenium based flat-panel detectors for digital mammography: Characterization of a small area prototype detector," *Med. Phys.*, vol. 30, no. 2, pp. 254–263, Feb. 2003, doi: 10.1118/1.1538233.

[3] D. C. Hunt, O. Tousignant, and J. A. Rowlands, "Evaluation of the imaging properties of an amorphous selenium-based flat panel detector for digital fluoroscopy," *Med. Phys.*, vol. 31, no. 5, pp. 1166–1175, May 2004, doi: 10.1118/1.1707755.

[4] L. Peng, L. Hu, and X. Fang, "Low-dimensional nanostructure ultraviolet photodetectors," *Adv. Mater.*, vol. 25, no. 37, pp. 5321–5328, Oct. 2013, doi: 10.1002/adma.201301802.

[5] T. Liu, J. Hu, Z. Jin, F. Jin, and S. Liu, "Two-photon ratiometric fluorescent mapping of intracellular transport pathways of pH-responsive block copolymer micellar nanocarriers," *Adv. Healthcare Mater.*, vol. 2, no. 12, pp. 1576–1581, Dec. 2013, doi: 10.1002/adhm.201200436.

[6] Y. El-Mohri, K.-W. Jee, L. E. Antonuk, M. Maolinbay, and Q. Zhao, "Determination of the detective quantum efficiency of a prototype, megavoltage indirect detection, active matrix flat-panel imager," *Med. Phys.*, vol. 28, no. 12, pp. 2538–2550, Dec. 2001, doi: 10.1118/1.1413516.

[7] H. Jiang, Q. Zhao, L. E. Antonuk, Y. El-Mohri, and T. Gupta, "Development of active matrix flat panel imagers incorporating thin layers of polycrystalline HgI2 for mammographic x-ray imaging," *Phys. Med. Biol.*, vol. 58, no. 3, pp. 703–714, Jan. 2013, doi: 10.1088/0031-9155/58/3/703.

[8] Y. El-Mohri *et al.*, "Active pixel imagers incorporating pixel-level amplifiers based on polycrystalline-silicon thin-film transistors," *Med. Phys.*, vol. 36, no. 7, pp. 3340–3355, Jul. 2009, doi: 10.1118/1.3116364.

[9] S. O. Kasap and J. A. Rowlands, "Direct-conversion flat-panel X-ray image sensors for digital radiography," *Proc. IEEE*, vol. 90, no. 4, pp. 591–604, Apr. 2002, doi: 10.1109/JPROC.2002.1002529.

[10] F. Taghibakhsh and K. S. Karim, "Two-transistor active pixel sensor readout circuits in amorphous silicon technology for high-resolution digital Imaging applications," *IEEE Trans. Electron Devices*, vol. 55, no. 8, pp. 2121–2128, Aug. 2008, doi: 10.1109/TED.2008.926744.

[11] M. Simon *et al.*, "Analysis of lead oxide (PbO) layers for direct conversion X-ray detection," *IEEE Trans. Nucl. Sci.*, vol. 52, no. 5, pp. 2035–2040, Oct. 2005, doi: 10.1109/TNS.2005.856790.

[12] R. A. Street *et al.*, "Comparison of PbI_2 and HgI_2 for direct detection active matrix X-ray image sensors," *J. Appl. Phys.*, vol. 91, no. 5, pp. 3345–3355, Feb. 2002, doi: 10.1063/1.1436298.

[13] S. Adachi *et al.*, "Experimental evaluation of a-Se and CdTe flat-panel X-ray detectors for digital radiography and fluoroscopy," in *Proc. SPIE*, vol. 3977. San Diego, CA, USA, Apr. 2000, p. 38, doi: 10.1117/12.384511.

[14] A. K. Maki1, J. G. Mainprize, and M. J. Yaffe, "Technical note: Robust measurement of the slice-sensitivity profile in breast tomosynthesis," *Med. Phys.*, vol. 43, no. 8, p. 4803, Aug. 2016, doi: 10.1118/1.4959539.

[15] M. Schieber, A. Zuck, H. Gilboa, and G. Zentai, "Reviewing polycrystalline mercuric iodide X-ray detectors," *IEEE Trans. Nucl. Sci.*, vol. 53, no. 4, pp. 2385–2391, Aug. 2006, doi: 10.1109/TNS.2006.877043.

[16] F. Taghibakhsh and K. S. Karim, "Two-transistor active pixel sensor for high resolution large area digital X-ray imaging," in *IEDM Tech. Dig.*, Washington, DC, USA, Dec. 2007, pp. 1011–1014, doi: 10.1109/IEDM.2007.4419126.

[17] H. Gilboa *et al.*, "Medical imaging with mercuric iodide direct digital radiography flat-panel X-ray detectors," in *Proc. SPIE*, vol. 4784. Seattle, WA, USA, Jan. 2003, p. 315, doi: 10.1117/12.450503.

JAE CHUL PARK received the Ph.D. degree from the Institute of Physics and Applied Physics, Yonsei University, South Korea, in 2014. He has been working as a Senior Researcher with the Samsung Advanced Institute of Technology since 2006.

SEUNG-EON AHN received the Ph.D. degree in electrical engineering from Korea University, South Korea, in 2013. He was with the Samsung Advanced Institute of Technology, Giheung, South Korea, from 2005 to 2015. He is currently an Assistant Professor with the Department of Nano-Optical Engineering, Korea Polytechnic University, South Korea.